COMPARISON OF POLAR AND EQUATORIAL MAGNETIC FIELDS NEAR SUNSPOT MINIMUM

L. D. ZHANG, H. ZIRIN and W. H. MARQUETTE
Big Bear Solar Observatory, California Institute of Technology, Pasadena, CA 91125, U.S.A.

(Received 10 January 1997; accepted 21 February 1997)

Abstract. We investigate the polar magnetic fields near sunspot minimum using high-resolution videomagnetograph data from Big Bear Solar Observatory. To avoid the problem of center-to-limb variation of the projected longitudinal field, we compare polar with equatorial field strengths for the same limb distance. Polar fields are stronger than the quiet equatorial field, but no greater than equatorial limb data containing unipolar regions. The difference is entirely in the stronger field elements. The polar background fields are of mixed polarity but show a net weak field opposite in sign to that of the stronger polar elements. We believe this to be the first evidence of widespread background field. No dependence of the measured signal on the B-angle was found, so the high-latitude fields do not change strength near the pole. Further, there was no significant change in the polar fields in the 15-month period studied. We tried to derive a high-latitude rotation rate; our data show motion of high-latitude magnetic elements, but the diurnal trajectory is not much bigger than random motions and field changes, so the result is inconclusive. We suggest that the polar fields represent the accumulation of sunspot remnants, the elements of which last for years in the absence of other fields.

1. Introduction

The polarity reversal of the Sun's polar magnetic fields around sunspot minimum remains a mystery, despite the formulation of phenomenological models to explain the process (Murray and Wilson, 1992; Lin, Varsik, and Zirin, 1992). At Big Bear Solar Observatory high-resolution polar magnetic observations are regularly obtained to understand the reversal process (Tang and Wang, 1991; Lin, Varsik, and Zirin, 1994). We have studied the polar fields near sunspot minimum with the following objectives: (1) to determine if the polar fields are stronger than the general quiet-Sun fields, and (2) to investigate the dynamics of the polar fields, including the motion of magnetic field pattern due to high-latitude rotation.

One of the salient aspects of the solar magnetic cycle is the concentration of unipolar magnetic fields at the poles at sunspot minimum. Not only is unipolar field concentrated at the pole, but it appears to be stronger than the equatorial fields. Like the other quiet-Sun fields, the polar fields really consist of a network of strong individual magnetic elements superposed on a mixed background of weak intranetwork (IN) fields (Tang and Wang, 1991; Lin, Varsik, and Zirin, 1994). Because the polar field signal is weakened by projection, the IN fields are very hard to detect and will play a minor role in our discussion. The mechanism of concentration and polarity reversal was first addressed by Leighton (1964, 1969), and later by Sheeley and his coworkers (DeVore, Sheeley, and Boris, 1984; Sheeley,

Solar Physics **175:** 59–80, 1997.

Nash, and Wang, 1987; DeVore and Sheeley, 1987; Wang, Nash, and Sheeley, 1989). None of these models explains how the peak field intensities at the pole can exceed those at the equator (if indeed they do), or how the flux elements survive the long journey from equator to pole. Other than the apparent polar excess, the strength of the polar fields compared to the equatorial was not known. The random-walk diffusion constant required for Leighton's model is in fact much greater than actually observed (Mosher, 1977).

The true intensity of fields near the pole is difficult to determine. Most of the photospheric magnetic fields emerge normal to the Sun's surface (Howard and LaBonte, 1981). Since current magnetographs are only sensitive enough in the longitudinal mode to measure these quiet-Sun fields, the line-of-sight component of the Zeeman signal of the polar fields is difficult to measure. In general, the measured field strength should be multiplied by the secant of the heliocentric angle (or the viewing angle of the surface from the observer). But Murray (1992) has shown that this correction holds for fields within 70° of Sun center. But the failure of the cosine dependence in his case was due to his use of full-disk magnetograms with low signal-to-noise values near the extreme limb. Since the equatorial field strengths are roughly independent of longitude when no activity is present (especially at sunspot minimum), the attenuation of the apparent signal with heliocentric angle is derived by comparison with disk-center measurement, and finally equatorial and polar limb data are compared to determine the excess, if any, of polar over equatorial fields. In this way we determine the ratio of polar to equatorial fields for any heliocentric angle.

2. The Observational Data

Polar data has been obtained at BBSO for some years, typically about three days a month. As time went by it was found worthwhile to take an expanding series of data. In recent years the minimum set has been two magnetograms at each pole, two at an equatorial limb (after checking which limb is the quietest) and one at Sun center. Sometimes this was expanded to cover a larger part of the polar regions. The Sun-center magnetogram permits cross-calibration with other magnetographs. The magnetograms are composed of 4096 frames, half in each circular polarization. Most of the data presented here is the average of two consecutive videomagnetograms (VMGs). The mean noise per pixel (Figure 1) is ± 1.5 G per pixel, but since each magnetic element has roughly 25 pixels, it is about ± 0.3 G per magnetic element. In addition there is a frame-to-frame fluctuation of about 0.3 G. The field of view is 3.5×5 arc min. Data from six good days were chosen for analysis. The BBSO magnetograms use a detector of spatial resolution $0.56''$ per pixel in the x direction and $0.46''$ per pixel in the y direction. However, the integration over 4096 frames spreads the image out to about 2 arc sec (actual spatial resolution). Only data of good seeing were selected. Care was taken to use equatorial data free of

sunspot activity. The Caltech videomagnetograph operates at the Ca I 6102.727 Å absorption line (Mosher, 1976; Zirin, 1985). Because of equatorial rotation, the central wavelength is adjusted for Doppler shift at the limb (increased or decreased by 0.04 Å for the west or the east limb respectively).

A detailed account of the calibration of the videomagnetograph is presented by Varsik (1995). He showed a Big Bear VMG with an NSO active region magnetogram taken at the same time. Except for slight seeing variation the two are identical. Despite the claims of Lites, Pillet, and Skumanich (1994), who suggest that videomagnetograms are in error by 30%, magnetograms taken 1000 miles apart by two different techniques match perfectly and the internal consistency of the data shows them to be accurate, dependable and highly sensitive. The frame-to-frame variation of successive magnetograms is about 0.25 G or less. The true field intensity is of course affected by seeing, but the flux of an element is not. Varsik also found the calibration of the magnetograph to have a mean dispersion around $\pm 7\%$ over several years. The data he surveyed went up to 1993; since then the instrument has been even more stable. The stability since 1995 is discussed in the Appendix. A low-frequency filter is used to give a uniform response over the field.

One factor that cannot be dealt with by calibration is the effect of seeing, which varies from day to day. Just as one can argue the existence of kilogauss fields in the quiet Sun that are masked by the filling factor (Stenflo, 1973), measurement of the peak intensity of any structured field will be affected by the spatial resolution of the system. Not only the peak field strength but the total field in an element will be affected, since diffuse signal disappears in the noise. Also, because the strongest elements contribute the most to pole-equator asymmetry, the seeing plays a role in minimizing their strength. We try to confirm absolute field measures by referring to the Sun center measurements. By choosing data with good seeing, we have minimized this effect. We try to normalize field measures by referring to the Sun center measurements.

Apart from active regions, detectable magnetic fields of the equatorial region can be divided into three categories (Zirin, 1988): quiet-Sun, unipolar magnetic regions (or enhanced network), and intranetwork (IN) fields (Zirin, 1985). It has not been established whether the last vary in strength with the first two. We have tried to compare the polar fields with either of the first two. We measured disk-center quiet magnetic regions for 23, 26 April and 2, 10 May, 1996, and enhanced network for 24 and 29 April, 1996. This data simply measures day-to-day variation. Unfortunately two of the six days of polar observation do not have quiet-Sun data, but Table I shows very little scatter. So the sensitivity was essentially constant through this period.

The present polar measurements use days for which comprehensive sets of data, including two measurements of each target on both poles and equatorial limbs, were obtained. The polar data for 23, 24, 26 April and 2, 3, 10 May, 1996 were analyzed. Quiet equatorial limb data for 14 February, 18 March, 24 and 29 April, and 15 May (two limbs) were used for comparison. We wanted the same day as the polar data

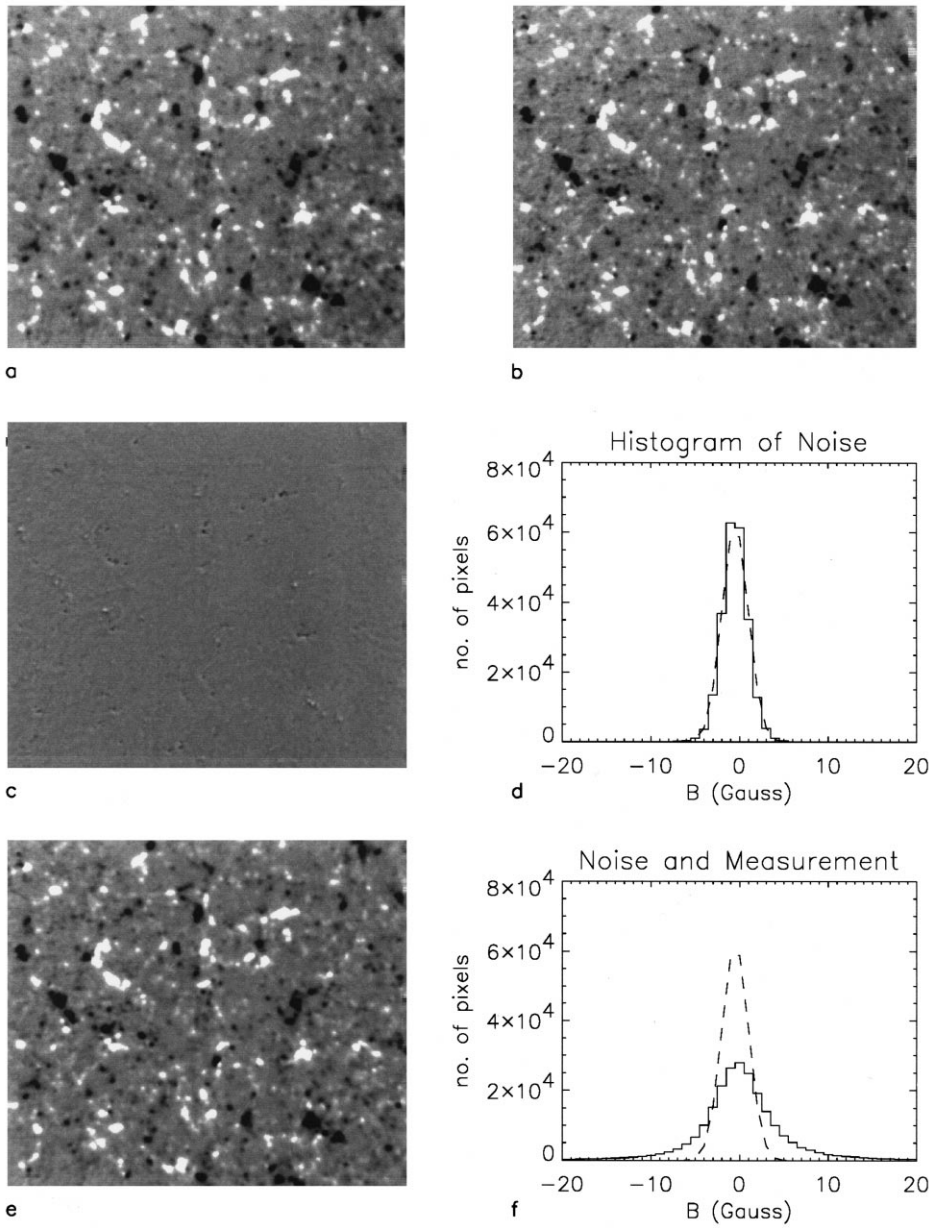

Figure 1. Images of the disk center and determination of the noise level. (a) and (b) are two consecutive magnetograms, separated by 4 min, of the same disk-center region; (c) is the image of $(a - b)/2$, a measure of the average random noise of the two. The histogram plot of the brightness distribution in (c) is shown in (d). The dashed line in (d) is a Gaussian fit to the noise. (e) is the image of $(a + b)/2$, i.e., the average of the two. (f) shows the Gaussian fit (dashed line) compared to the actual distribution of field in (e) (solid line). In either adding or subtracting of the two images, the second image is shifted to the left by one pixel to insure maximum correlation between the two images. The motion to the left is due to the rotation of the Sun.

Table I
Properties of disk-center fields

Type of fields	Unsigned mean flux density (G)	Fractional area of field above 2σ level (%)	Unsigned flux density in magnetic elements (G)
Quiet regions	4.66 ± 0.19	43.5 ± 1.6	9.5 ± 0.5
Unipolar magnetic regions	6.54 ± 0.06	44.9 ± 1.3	13.3 ± 0.2

Note that while the threshold for a single pixel is 2σ, for a magnetic element it is less. When a judgement is made of a magnetic feature detected on the magnetogram, one's eye has already integrated the values of at least 2×2 arc sec, or 4×4 pixels. The standard deviation of the mean of sixteen pixels is $\sigma/4$, and the 2σ noise level on this scale is $2\sigma/4$. So the field detection threshold on this scale is $\Sigma = \sigma/2$, about 1 G.

if possible, but if a unipolar region was present, we used the nearby days. In any event, except for Figure 3, we combined the data for all the days of the same type. The range of B_0 in the above polar data set is from -4.9° to -3.2°. Four days of enhanced regions near the limb were used: 23 April, 29 April, 2 May, and 3 May, 1996. Except for the amount of enhanced network present varying with solar rotation, there is little difference between these days. The Appendix also shows that there was little variation in seeing and calibration in the entire 12-month period. We use the data on 17, 22 June, 1995 for the north pole rotation measurement and 19, 20 June, 1995 for the south pole.

3. Noise Level and Properties of Disk-Center Fields

The noise in the magnetogram was estimated by subtracting two successive deep field magnetograms of the same region. Figure 1 shows a typical magnetogram of the disk center and a histogram plot of the distribution of magnetic field strength. Most of the fields measured are of apparent value less than 10 G. To determine the noise level, we take two magnetograms of the same disk-center region and then subtract the one image from another and divide the result by two. In this way we get a measure of the real noise for the superposed average of two magnetograms. Figure 1(d) is a histogram plot of the noise. We fitted the noise distribution in the pixels with a Gaussian distribution of standard deviation $\sigma = 1.5$ G.

We determined the following properties of the quiet disk center fields for the current phase of solar minimum: (1) unsigned mean flux density, the average absolute magnetic field strength distributed over the whole surface; (2) fractional area, the fraction of the pixels with magnetic field strength above the 2σ (3 G) level; (3) unsigned flux density in quiet magnetic elements, i.e., the average absolute field strength in all pixels above the 2σ threshold, in this case 3 G.

Because of the decreasing light intensity as one goes to the limb, the noise level in the magnetogram also goes up. Figure 2 shows a pair of equatorial limb mag-

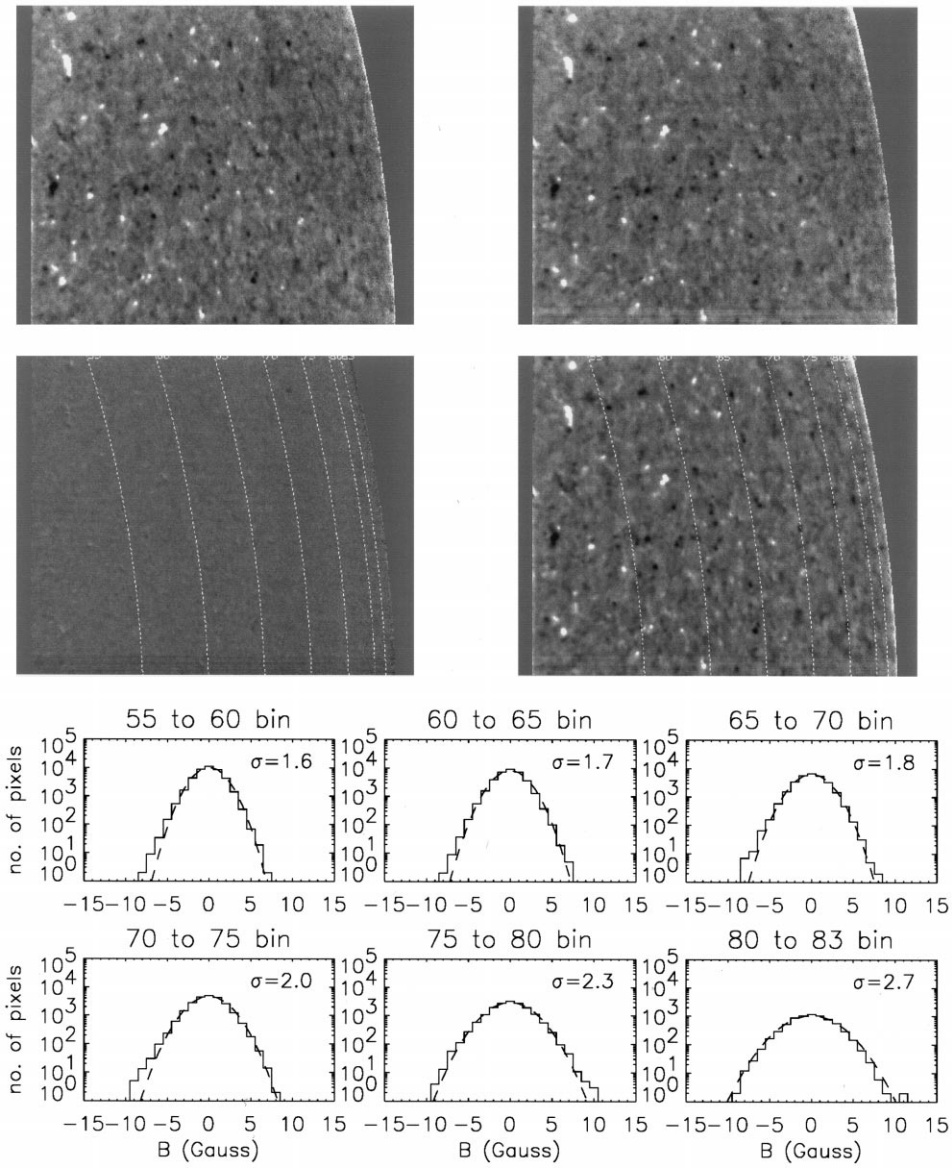

Figure 2. Two successive equatorial limb magnetograms (*top row*) with their difference and average (*second row*). Plots shown below are histograms of the difference image in bins of heliocentric angle which correspond to the noise. In each case we give the standard deviation of the Gaussian fit. The noise is larger than in Figure 1 because of limb darkening.

netograms, and their difference and sum, respectively, with concentric heliocentric distances shown in the latter. The noise level determined from the difference is plotted in the lower half as a function of the heliocentric angle. By fitting the noise histograms in each bin we found the standard deviations in Table II.

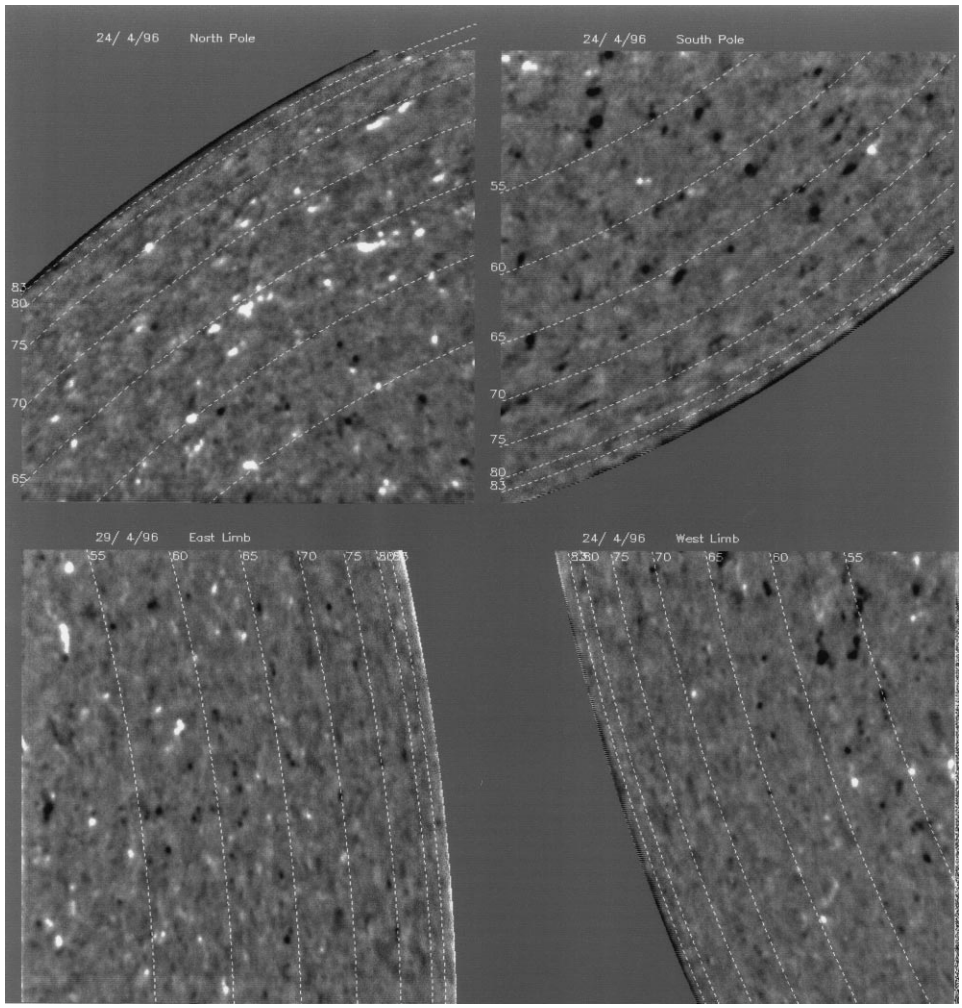

Figure 3. Comparison of the polar limbs and the west equatorial limb fields on 24 April, along with a VMG of the east limb on 29 April. We can easily see the higher field levels at the pole.

Table II
Noise level as a function of heliocentric angle

Bins	55–60	60–65	65–70	70–75	75–80	80–83
σ (G)	1.6	1.7	1.8	2	2.3	2.7

4. Comparison of Polar and Equatorial Limb Fields

Concentric lines are drawn on the polar and equatorial limb magnetograms (see Figure 3), so that one can compare the polar and equatorial region at approximately

Table III
Comparisons of the poles and the quiet equatorial limb

Heliocentric angle bins (deg)	Line-of-sight unsigned mean flux density (G)		Fractional area of fields above 2σ noise level (%)	
	Poles	EQ-limb	Poles	EQ-limb
55–60	2.70 ± 0.12	2.64 ± 0.13	26.4 ± 2.5	26.6 ± 1.9
60–65	2.79 ± 0.28	2.45 ± 0.37	25.0 ± 3.2	22.1 ± 4.5
65–70	2.68 ± 0.21	2.24 ± 0.19	23.0 ± 2.8	18.9 ± 3.3
70–75	2.55 ± 0.19	2.32 ± 0.22	18.8 ± 2.5	16.5 ± 3.7
75–80	2.57 ± 0.12	2.30 ± 0.17	14.3 ± 2.0	11.3 ± 2.6
80–83	3.01 ± 0.18	2.68 ± 0.31	12.0 ± 2.3	11.1 ± 3.9

equal heliocentric angle. Although the concentric lines do not coincide with the lines of equal latitude, the latitude variation within each bin of heliocentric angle is not significant. Therefore the values of heliocentric angle are approximately equal to the uncorrected values in apparent latitude (B_0).

We compare the polar data set with the quiet equatorial data set in the same bins of heliocentric angle. As mentioned above, each data set contains measurements of the region on six different days. Figure 3 compares the polar limbs and the west equatorial limb on 24 April, along with a videomagnetograph of the east limb on 29 April. We can easily see the higher field levels at the pole.

Results are given for line-of-sight unsigned mean flux density and apparent fractional area of line-of-sight magnetic fields above the pixel sensitivity in the following table. The noise figures for the flux density are essentially the day-to-day scatter, since the error for a full frame is very small.

Table III minimizes the differences because the main pole-equator effect is limited to the stronger elements. In Figures 4(a) and 4(b) we show the comparison of the averaged data for north pole versus equatorial limb and for south pole versus equatorial limb for different field strengths. Band $55^\circ - 60^\circ$ shows no difference between solid (pole) and dashed (equator) curves. Starting at 60° the two curves diverge, the separation increasing with field strength. The only exception is in the S pole data above 80°, which show no difference, probably because the signal is weak. This figure means that above 65° heliocentric angle, the stronger polar fields are 2–3 times more frequent than the equatorial. Another way of putting it is, 'the stronger equatorial fields disappear at field strengths half the corresponding level for the poles'. Since the latitude variation within each heliocentric degree bin on the magnetogram is not significant, we conclude that the area of strengthened polar fields is about 25° in latitude around the pole, a value that corresponds quite well with the size of the polar coronal hole observed in the UV during the same period.

The message of Figure 4 can be phrased in terms of ratio of probabilities, that is, the ratio of probabilities of finding measured line-of-sight fields in the range 10–20, 20–30, 30–40 G at the poles and the equatorial limb.

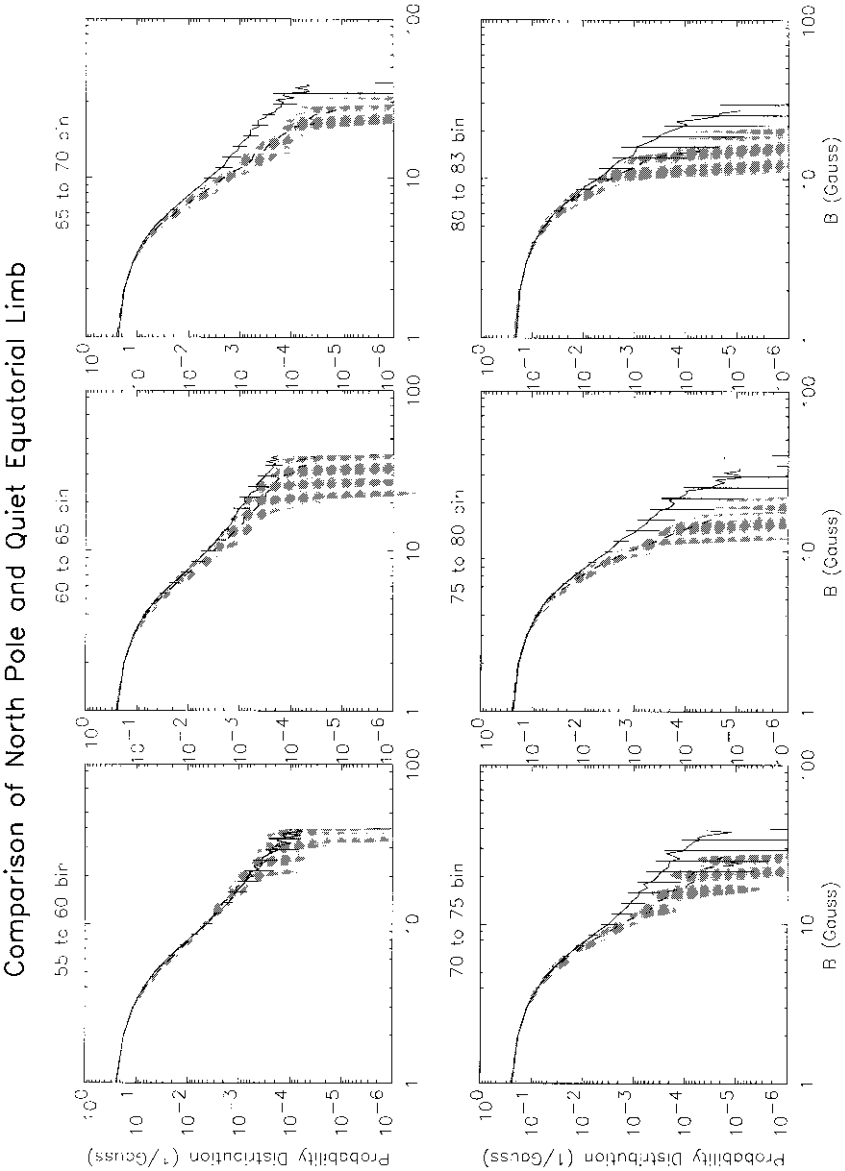

Figure 4a. Probability distributions of the north pole and quiet equatorial limb magnetic fields, using data taken on six different days. The solid line is the probability that the measured magnetic field in a pixel at the north pole falls in a one-gauss band at that abscissa. The dashed line gives the same probability for the equatorial data. The vertical bars are the standard deviation for the pole; the shaded regions are the same for the equatorial limb. The logarithmic display produces the asymmetry.

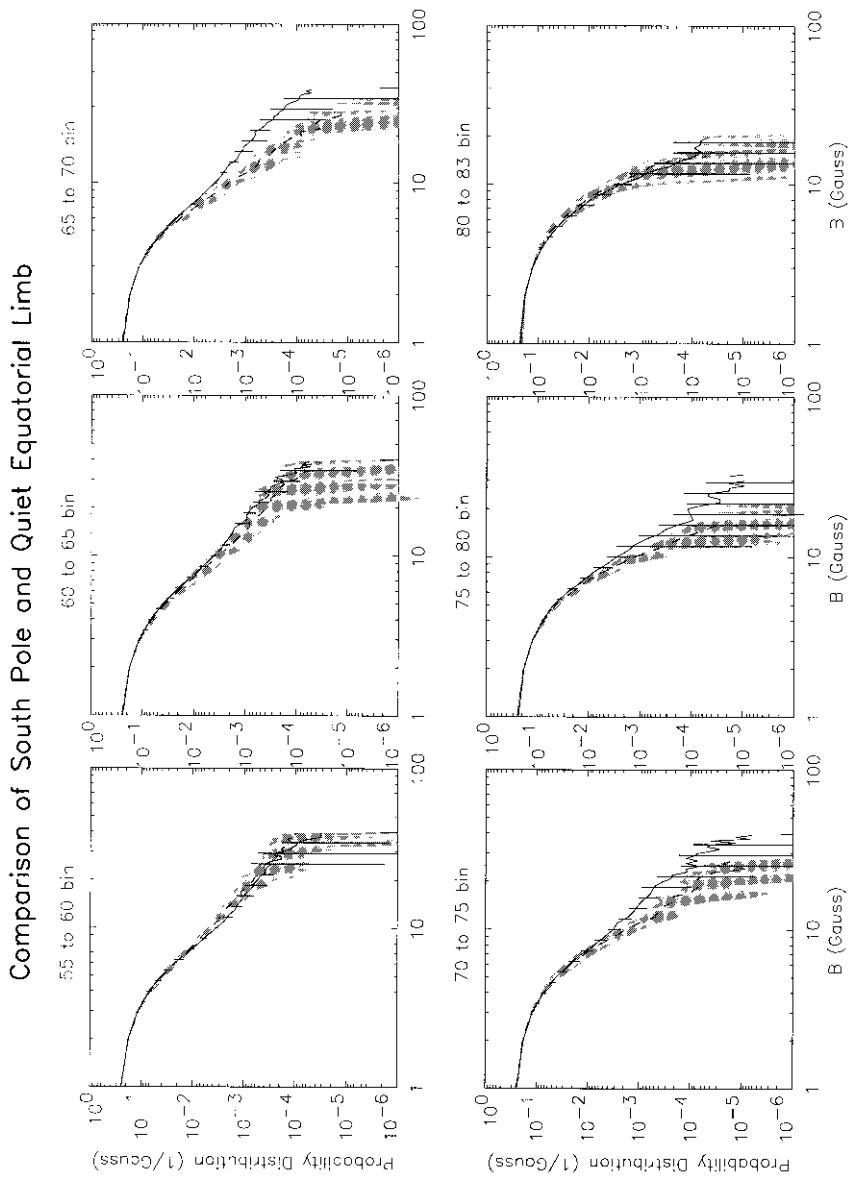

Figure 4b. Same plot as Figure 4(a) for the south pole and the equatorial limb.

Table IV
Ratio of probabilities between the poles and the equator

Degree bin		55–60	60–65	65–70	70–75	75–80	80–83
10–20 G	NP/EQ	0.8	1.5	2.7	2.7	4.4	2.6
	SP/EQ	0.7	1.4	3.0	2.7	3.1	0.8
20–30 G	NP/EQ	0.8	2.0	8.7	7.0	79.0	24.3
	SP/EQ	0.8	1.5	10.0	5.0	39.0	1.5
30–40 G	NP/EQ	0.7	3.4	38.8	∞	∞	0/0
	SP/EQ	0.4	1.6	39.5	∞	∞	0/0

Table IV summarizes the comparison, giving the above probabilities for different heliocentric angles and field strength bins. For example, in the heliocentric angle bin 75°–80°, it is about 80 times more likely to find measured fields in the range 20–30 G at the north pole than at the quiet equator! For measured fields of 30–40 G the ratio becomes infinite beyond 70° because the probability of finding these fields is zero at the quiet equator.

Until this point we have only compared the polar fields with quiet equatorial fields and they are clearly stronger. But there are often unipolar magnetic regions in low latitudes apart from active regions. In Figure 5 we compare the polar data for 24 November, 1996 with the E limb equatorial data for the same day including a unipolar region. The strong polar magnetic elements are similar to, but slightly weaker than, the enhanced network magnetic elements. In Figure 6 we plot this comparison following the method of Figure 4(a). We see that they are quite similar. Thus the fields away from active regions fall into two bins, quiet-Sun and unipolar enhanced network. Our data show that at sunspot minimum the poles are occupied by enhanced network. There also are occasionally regions of enhanced mixed polarity, but we do not see these moving to the poles. Our result supports the idea that the polar field is accumulated from the unipolar regions which are known to be the detritus of the strong fields in active regions. But this work sheds no light on how these fields reach the pole or how preceding or following polarities are separated. However, in all of our data we have seen no flux emergence and little bipolar flux in the polar regions, so the only source would appear to be the equatorial unipolar regions.

We have shown that at sunspot minimum, the magnetic fields at the poles are stronger than the normal quiet Sun, but roughly of the same strength as the unipolar regions that apparently result from the decay of active regions. A numerical and visual comparison of the polar and quiet equatorial limb images clearly shows the difference between the poles and the quiet equator (see Figure 3). The stronger magnetic elements found at the poles are absent at the quiet equatorial limb. Figure 4 and Table IV show us that the difference is most pronounced in the stronger field elements. The weaker elements show a surprising result.

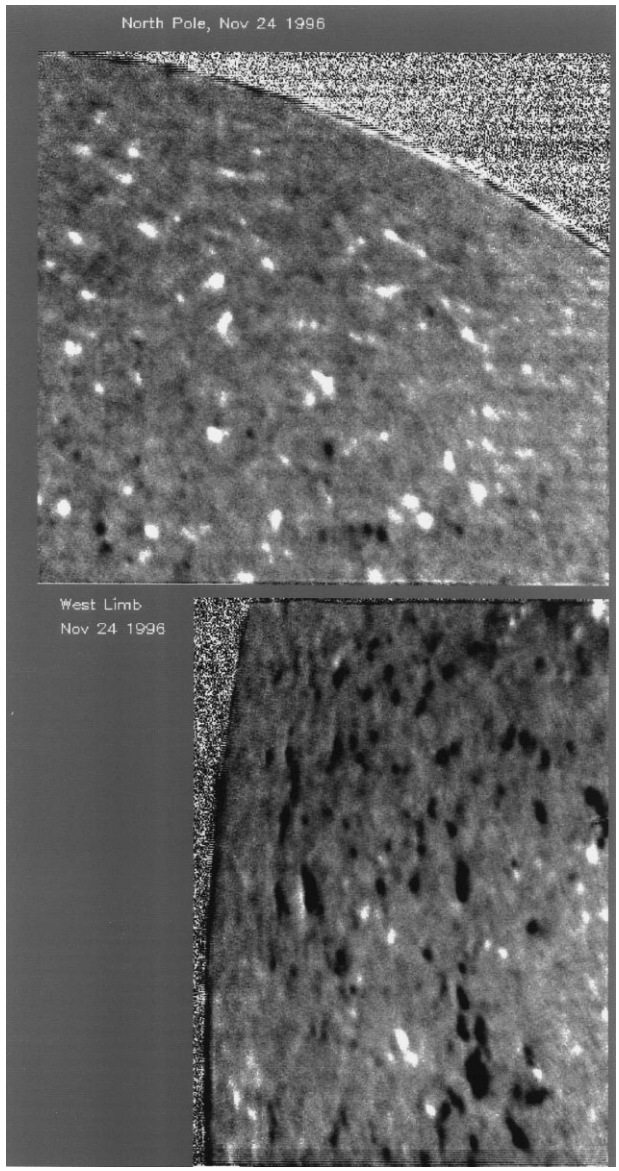

Figure 5. Comparison of polar and equatorial magnetograms on 24 November, 1996, when a unipolar region approached the limb. The stronger polar elements are similar to or slightly weaker in strength than the equatorial.

For some years we have had the impression that the background fields had a general net polarity opposite that of the stronger unipolar fields; we measured the net sign of all the weak polar fields below a varying threshold and compared these results with the average of the corresponding equatorial data. Figure 7 shows the average signed polarity of all pixels above 2σ and below certain limits at each pole

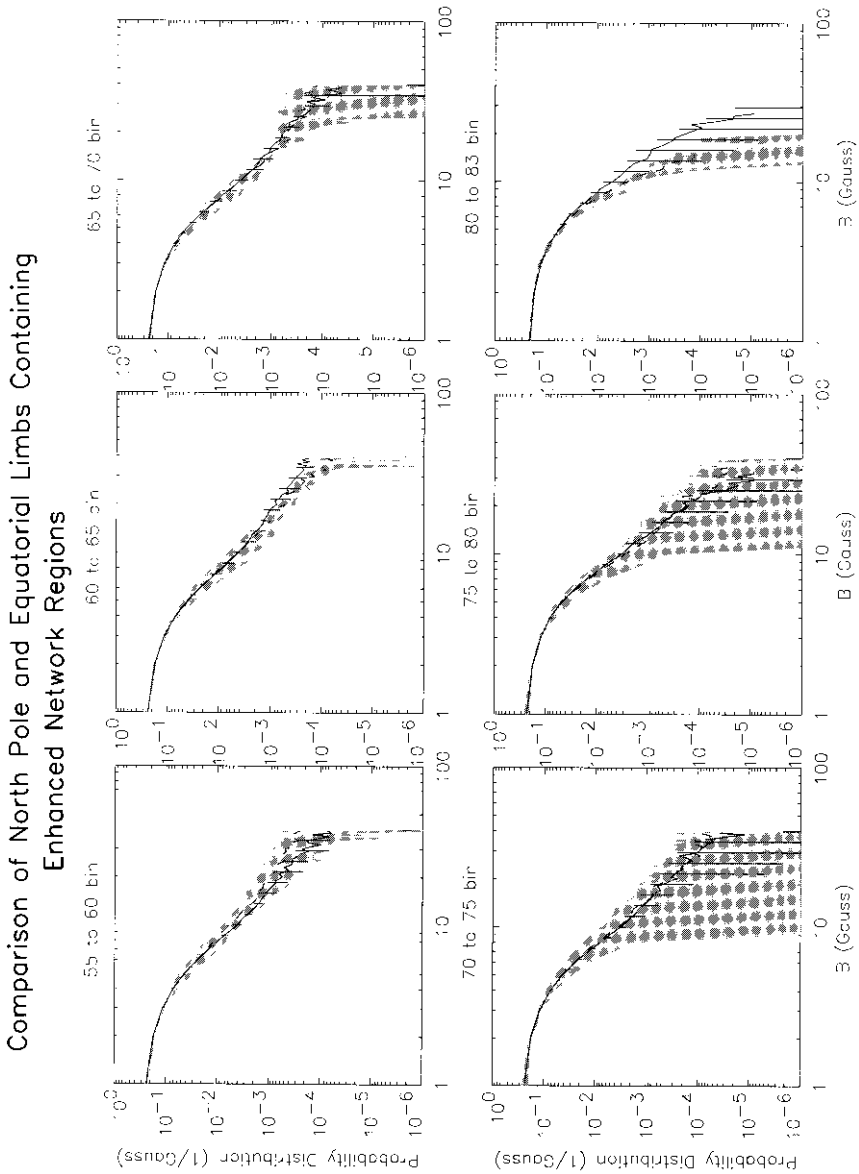

Figure 6. Similar to Figure 4 comparing polar data with equatorial containing unipolar regions.

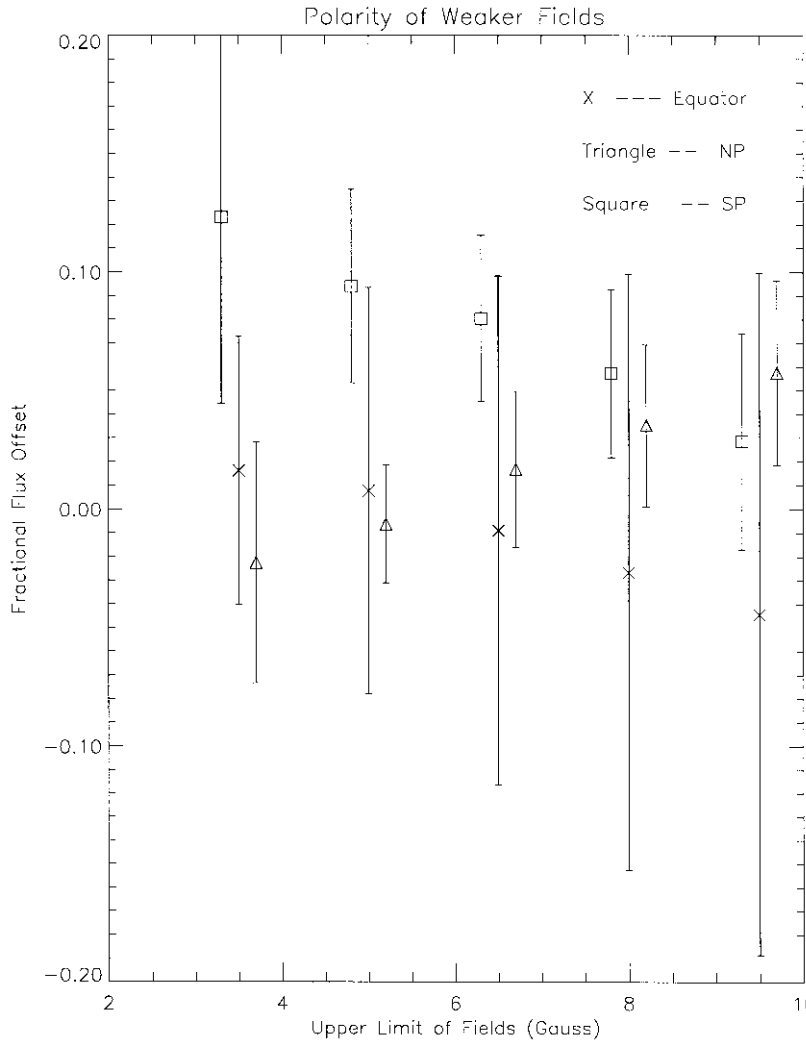

Figure 7. Average polarity of weaker fields at the pole and equator as a function of upper limit. In each case we measure only fields above a given upper limit, and we see that as this limit decreases, the offset of the weak fields increases. By contrast, the net signal of the equatorial weak fields is close to zero. The crossing of the north and the south pole at non-zero polarity value is due to the non-zero offset in the magnetogram. Normally, the modulator is adjusted so that zero field is at pixel value 128; but in this case there is an offset of 0.05 G on the average. The reality of the effect is demonstrated by the inverse symmetry of the signals from the opposite poles. The equatorial data shows no such effect.

and the equatorial limb. While the measurement in any bin is quite noisy, there is a definite pattern. The net polarity is given as a fraction the average field strength and is not zero, and the effect clearly increases as we sample bins of lower and lower field strength by decreasing the upper level (the fields below 2σ average out to 0

by definition). At the opposite pole, the conjugate result is found; the weak fields have a net polarity opposite the stronger fields (which still dominate the overall net result). By contrast, the equatorial limb fields show a much smaller net polarity, zero within the error bars. We checked several equatorial unipolar regions for the possibility that instrumental effects balance the background against the dominant field, and found no net field in the background of those. Thus the effect is real and limited to the poles. It is the first detection of diffuse (non-dumped) fields on the Sun (it is difficult to prove this fact, but visual inspection as well as the ratio of the net to the total flux supports it). It may be that some of the polar fields return to the nearby surface in more diffuse patterns. To be sure, the net flux for all field strengths remains the same sign as the stronger elements, but the structure is not exactly unipolar. The exact topology of the field lines of the strong polar magnetic elements is not known, i.e., we do not know where they return to the surface. The existence of a coronal hole at the pole tells us the field lines extend very far, but some may return. We plan to check data for earlier minima. The average field in the lower limit is 0.1−0.2 G; if the polar cap is 200 000 km across, the net flux is 3×10^{19} Mx, about the flux in a strong network element.

We have repeated these measurements on recent data and found the same effect. Furthermore we can exclude systematic error by switching the polarity of the modulator and find the signal reverses, showing that it is real.

5. Other Effects

With a calibrated set of polar data, we were able to study other properties of the polar fields. We measured the data from about May 1995 until June 1996 to see if there is any general change in the field, or if there is any dependence on the B angle. In both cases the conclusion is negative. In Figure 8 we plot the net flux as a function of time. Since the day-to-day scatter is a few tenths of a gauss, there is no discernible effect. Similarly, there was no obvious dependence on the B angle. Since the measurements above 80° are marginal, we must use favorable B angles to detect a possible change in field at the pole itself. This would appear as a systematic seasonal variation. But this does not appear to be present either, even in the high-latitude bands. Thus, there is no change in the field at latitudes above 83°. This can be seen from the magnetogram of the pole which appeared as a *Solar Physics* frontispiece (Zirin, 1995), which shows no apparent difference from the other polar fields.

Due to the discrepancy between the proposed polar spin-up of rotation of magnetic features and polar crown filaments (Stenflo, 1989; Brajša *et al.*, 1991) and the slower rates from helioseismology data (Woodard and Libbrecht, 1993), we take great interest in the rotation rate of the polar magnetic elements. While the fields can be followed throughout the day, it is virtually impossible to identify any features the next day. Further, the changes in shape of each feature during the 3-day limit

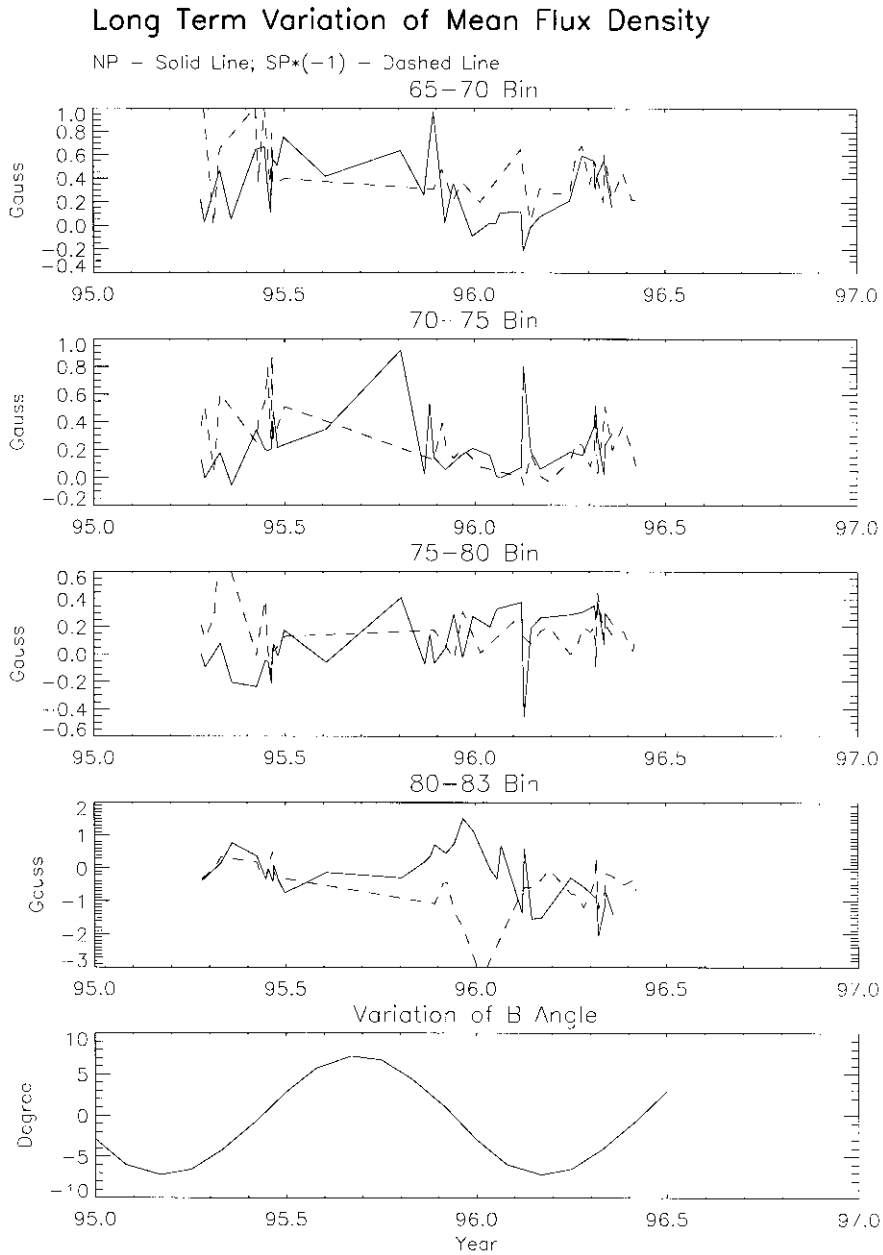

Figure 8. The net field (counting only data above 2σ) at either pole as a function of time. This shows generally little effect (except very low values at the beginning of 1996), that is, the changes over 18 months were small, of the order of 0.3 G, and there was no further variation in the extreme polar fields.

the length of the baseline. To measure the rate of high-latitude rotation of magnetic features, one has to continuously take magnetograph measurements of the same region for as many hours as possible within one day. Unfortunately this method is limited by declining seeing at the end of the day. It is also limited by the random motions and changes in the polar field elements, which are a significant fraction of the rotational motion. However, the direct measurement of rotational displacement appears to us more reliable than the method of autocorrelation analysis of magnetic tracers (Stenflo, 1989), because we have found no significant correlation from one day to the next.

The rotation rate of high-latitude magnetic features was determined by measuring the motions of the polar magnetic elements in a period of typically one to several hours. Measuring the motion of the elements in a longer time span, say one day, is practically impossible because the shape and size of the elements are completely changed in that period. We show in Figure 9 three polar magnetograms of the same region, separated by two hours in time. Eight elements were chosen at different latitudes and the rotation measured relative to the grid. The results are rather noisy but give limits on the rotation.

After carefully measuring the rotational motions of the magnetic elements on four different days (17, 19, 20, and 22 June, 1995), we determined the high-latitude rotation rates for magnetic elements as in Figure 10. The values of rotation rates below about 60° heliographic latitude are in good agreement with the general consensus (Gilman, 1974; Howard, 1984). However above 60° one might deduce a spin-up in the south pole data, although there is a large scatter in the rotation rates.

In the process of investigating the transient properties of polar magnetic elements, we have found several instances of a single magnetic element of opposite flux appearing on the polar magnetogram without the corresponding element of opposite sign. Since flux emergence on the surface of the Sun should occur in the form of dipoles (Zwaan, 1987), and emergence of a magnetic monopole is theoretically impossible, we should only see emergence or disappearance in conjugate pairs. An instance of this unexplained event appears in Figure 9. The negative magnetic element labeled as 'A' in the center magnetogram appears with no apparent opposite-polarity counterpart. Although it is hard to detect new positive polarity in a background of similar fields, the data are quite complete, and the surrounding magnetic fields show no apparent difference between the top and the center magnetogram. A possible explanation is that the field lines in the single element come back to the nearby surface in hardly detectable diffuse patterns. This hypothesis is not without reason because we have shown above that some of the strong polar magnetic fields may return to the surface this way. On the other hand we can see no evidence for such a return here.

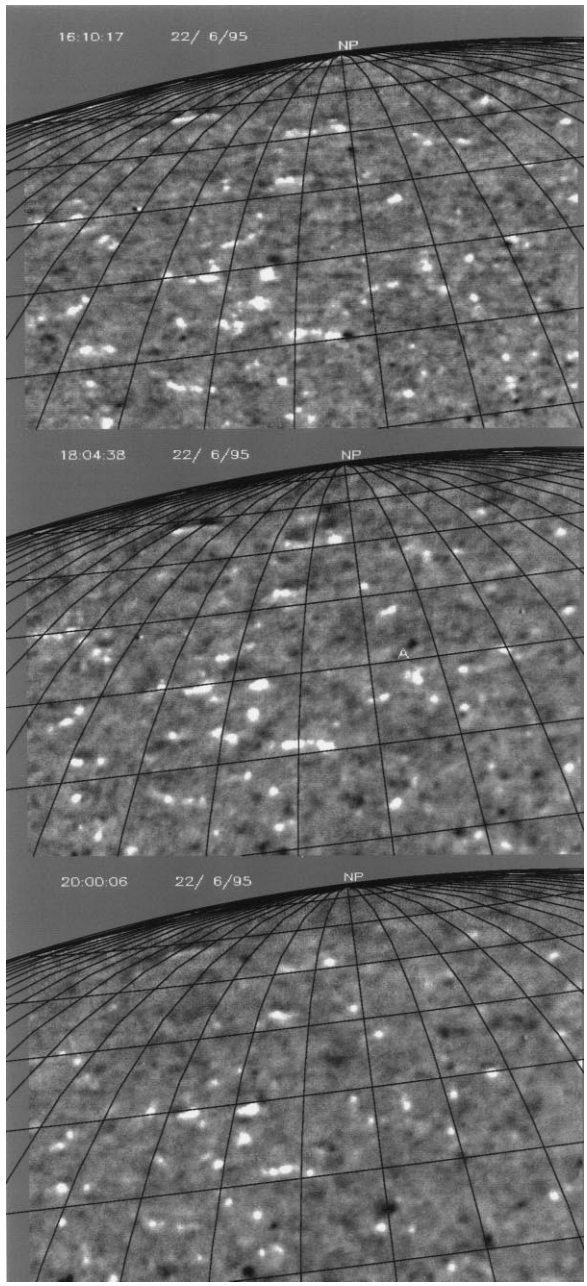

Figure 9. An example of three magnetograms on the same day on which a polar movie was taken. Lines of equal latitude and longitude are drawn on the magnetogram, each of which is separated by 5°. Therefore any motion of the elements is discernible over a span of several hours.

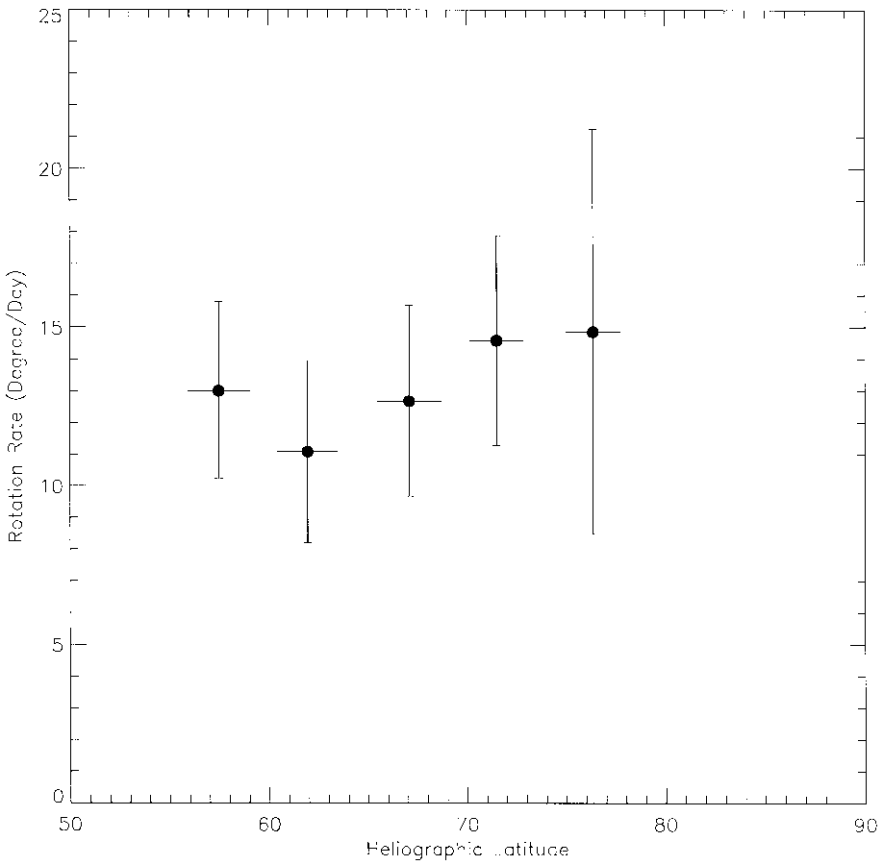

Figure 10. Measured rotation rate of high-latitude magnetic elements. The data are taken from polar observations on 17, 19, 20 and 22 June, 1995.

6. Conclusions and Discussion

We have systematically investigated the properties of the polar magnetic fields near sunspot minimum. Because the center-to-limb variation of the longitudinal magnetic signal is not securely established, the polar and equatorial limb were compared at the same heliocentric distances. Several different measurements showed the fields in the stronger polar elements ($B_{\rm obs} > 6$ G) to be 2–4 times more intense than equatorial counterparts. This results in an average field which similarly exceeds the equatorial. Analysis of the weaker polar fields shows a net field of about 0.07 G, with sign opposite to the strong polar elements at either pole. This suggests that at least some of the field lines of the polar elements return to the nearby surface in diffused patterns. We find that elements of equatorial unipolar regions are only slightly stronger than the polar elements.

Second, we found no explicit dependence of the polar fields on time or B_0 over a 15-month period. We measured the high-latitude rotation rates of magnetic elements and found the large scatter in the data exceeded any systematic effect, contradicting suggestions of a high-latitude spin-up. We found several cases of unipolar flux emergence, apparently in violation of Maxwell's laws.

The study of the apparent strength of the polar elements was undertaken to establish that they were indeed stronger than the quiet-Sun fields and then to understand how this may come about. We have now definitely established that this is true and that these fields are comparable to the unipolar elements of the enhanced network. That means that a circulation along the lines of Leighton's model or the Wang and Sheeley variant may take place. But clearly the magnetic elements must last for years. Since there has been little equatorial activity in recent years, the arrival of new field at the poles has surely ceased and the lack of change in the last year shows that the elements present at the beginning of 1995 are still there. We shall watch carefully as activity returns to see if the decline of the polar fields is due to decay or the advection of following polarity from the new cycle regions.

Acknowledgements

We would like to thank the staff at the Big Bear Solar Observatory for taking the data, especially Anders Johannesson who has provided the program of video-magnetograph flat fielding. The work is supported by ONR grant N00014−97−1−0080, NSF grant ATM-9525971, and NASA grant NAGW-1972.

Appendix. Long-Term Variability of BBSO Videomagnetograph Data

The atmospheric seeing conditions at the BBSO vary with the seasons, the best seeing coming in summer. Also there is a small random drift of the instrument (Varsik, 1995). So, even though the magnetograph is regularly calibrated, we need a standard reference field to compare magnetograph data from different periods. For this reason the mean flux density of the quiet disk center is observed with the polar data. This assumes that mean flux density of the quiet disk center is independent of the level of solar activity which may be quantified as the sunspot number.

We have compiled a data set from the beginning of 1995 until present. Visual inspection is applied to each image in selecting the data. It needs to be pointed out that in selecting both the polar data of this paper and the disk center data in this appendix we have used a uniform standard: that in IDL data display environment when one displays the image of the magnetogram in the byte scale range $(-20, 20)$, magnetic elements of all sizes are visible (during poor seeing conditions only the strong elements are visible), and that unipolar regions are not present.

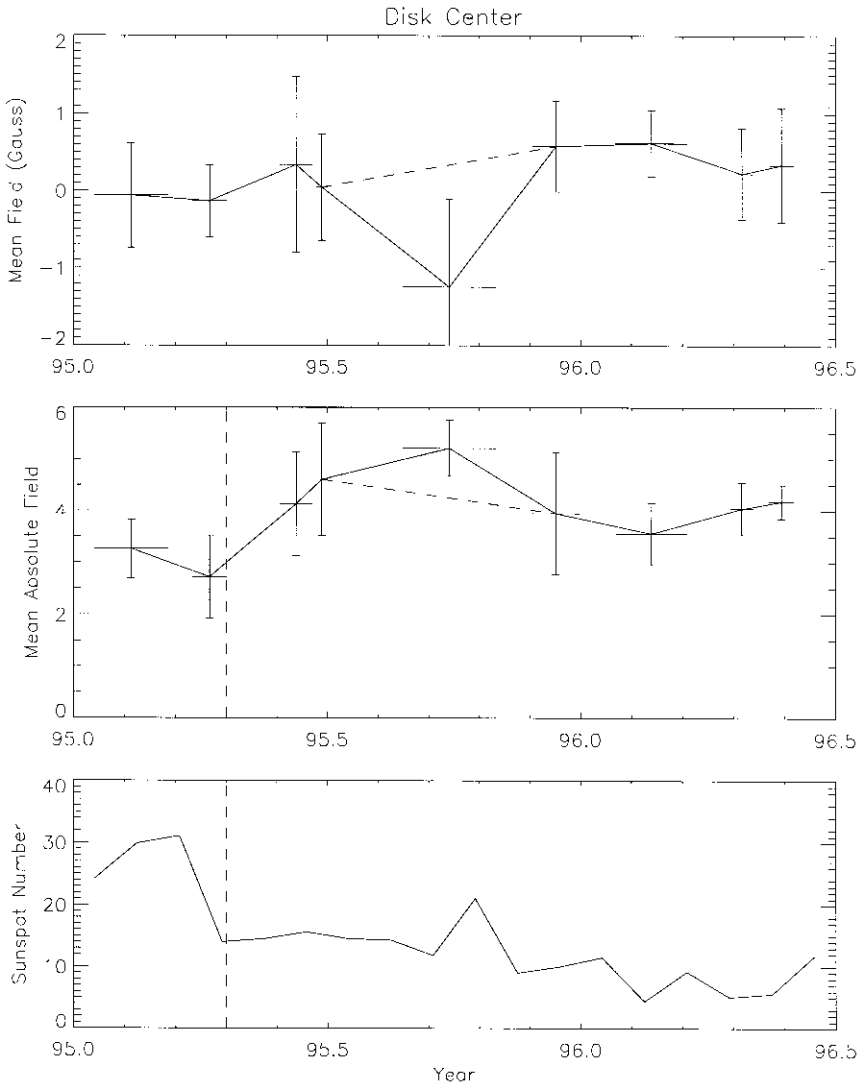

Figure 11. A check on the long-term variability of the BBSO magnetogram data. To the right of the dashed line (around May 1995) the level of solar activity is fairly constant, except for one point around October 1995 which also corresponds to a unipolar excess in the disk-center field. The mean absolute field of the disk center after May 1995 is also fairly constant except for one point which has a unipolar excess. The constancy of the mean absolute field suggests that there is no need of correcting for variations of calibration and seeing conditions.

In Figure 11 we have plotted the mean field and the mean absolute field of the disk center from the beginning of 1995 until the latest period. At the bottom is a sunspot number plot to indicate the level of solar activity. This number was rather constant from May of 1995 until the middle of 1996, except for a narrow surge of

activity during October 1995, which possibly is the cause of the unipolar excess of the disk center during the same period.

The mean absolute field is fairly constant except for one data point which has a unipolar excess. Therefore we conclude that for data from May 1995 until present we do not have to correct for the variation of calibration and seeing conditions.

References

Brajša, R., Vršnak, B., Ruždjak, V., Schroll, A., Pohjolainen, S., Urpo, S., and Terasranta, H.: 1991, *Solar Phys.* **133**, 195.
DeVore, C. R. and Sheeley, N. R. Jr.: 1987, *Solar Phys.* **108**, 47.
Devore, C. R., Sheeley, N. R., Jr., and Boris, J. P.: 1984, *Solar Phys.* **92**, 1.
Gilman, P. A.: 1974, *Ann. Rev. Astron. Astrophys.* **12**, 47.
Howard, R. F.: 1984, *Ann. Rev. Astron. Astrophys.* **22**, 131.
Howard, R. F. and LaBonte, B. J.: 1981, *Solar Phys.* **74**, 131.
Leighton, R. B.: 1964, *Astrophys. J.* **140**, 1547.
Leighton, R. B.: 1969, *Astrophys. J.* **156**, 1.
Lin, H., Varsik, J., and Zirin, H.: 1994, *Solar Phys.* **155**, 243.
Lites, B., Pillet, V. M., and Skumanich, A.: 1994, *Solar Phys.* **155**, 1.
Mosher, J.: 1976, BBSO Preprint series No. 0159.
Mosher, J.: 1977, Ph.D. Thesis, Caltech.
Murray, N.: 1992, *Astrophys. J.* **401**, 386.
Murray, N. and Wilson, P. R.: 1992, *Solar Phys.* **142**, 221.
Sheeley, N. R., Jr., Nash, A. G., and Wang, Y. M.: 1987, *Astrophys. J.* **319**, 481.
Stenflo, J. O.: 1973, *Solar Phys.* **32**, 41.
Stenflo, J. O.: 1989, *Astron. Astrophys.* **210**, 403.
Tang, F. and Wang, H.: 1991, *Solar Phys.* **132**, 247.
Varsik, J. R.: 1995, *Solar Phys.* **161**, 207.
Wang, Y. M., Nash, A. G., and Sheeley, N. R., Jr.: 1989, *Science* **245**, 681.
Woodard, M. F. and Libbrecht, K. G.: 1993, *Science* **260**, 1778.
Zirin, H.: 1985, *Aust. J. Phys.* **38**, 961.
Zirin, H.: 1988, *Astrophsics of the Sun*, Cambridge University Press, Cambridge, p. 124.
Zirin, H.: 1995, *Solar Phys.* **156**, 204 (frontispiece).
Zwaan, C.: 1987, *Ann. Rev. Astron. Astrophys.* **25**, 83.